Geomechanics and Engineering, *Vol. 36, No. 2 (2024) 131-143*
https://doi.org/10.12989/gae.2024.36.2.131

Pipeline deformation caused by double curved shield tunnel in soil-rock composite stratum

Ning Jiao[a], Xing Wan[b], Jianwen Ding*, Sai Zhang[c] and Jinyu Liu[d]

Institute of Geotechnical Engineering, School of Transportation, Southeast University, No.2, Southeast Road, Jiangning District, Nanjing, 211189, China

(*Received August 2, 2022, Revised December 8, 2023, Accepted December 11, 2023*)

Abstract. Shield tunneling construction commonly crosses underground pipelines in urban areas, resulting in soil loss and followed deformation of grounds and pipelines nearby, which may threaten the safe operation of shield tunneling. This paper investigated the pipeline deformation caused by double curved shield tunnels in soil-rock composite stratum in Nanjing, China. The stratum settlement equation was modified to consider the double shield tunneling. Moreover, a three dimensional finite element model was established to explore the effects of hard-layer ratio, tunnel curvature radius, pipeline buried depth and other influencing factors. The results indicate the subsequent shield tunnel would cause secondary disturbance to the soil around the preceding tunnel, resulting in increased pipeline and ground surface settlement above the preceding tunnel. The settlement and stress of the pipeline increased gradually as buried depth of the pipeline increased or the hard-layer ratio (the ratio of hard-rock layer thickness to shield tunnel diameter within the range of the tunnel face) decreased. The modified settlement calculation equation was consistent with the measured data, which can be applied to the settlement calculation of ground surface and pipeline settlement. The modified coefficients *a* and *b* ranged from 0.45 to 0.95 and 0.90 to 1.25, respectively. Moreover, the hard-layer ratio had the most significant influence on the pipeline settlement, but the tunnel curvature radius and the included angle between pipeline and tunnel axis played a dominant role in the scope of the pipeline settlement deformation.

Keywords: double curved shield tunneling; field monitoring; numerical simulation; pipeline deformation; soil-rock composite stratum

1. Introduction

With the acceleration of urbanization, the development and utilization of underground space has became the very important factor affecting the sustainable development of society (Jeon *et al*. 2020). Owing to advantages of high efficiency and little construction noise, shield tunneling has become the most popular method in urban tunnel construction (Koyama 2003, Jin *et al*. 2018, Xue *et al*. 2019, Qian *et al*. 2021). Notably, most urban shield tunnel crosses the areas with densely distributed underground pipelines, inevitably leading to the uneven settlement of grounds and the adjacent pipelines (Marshall *et al*. 2010, Zhang *et al*. 2016). Excessive pipeline deformation would exceed the bearing capacity of underground pipelines, which may threaten the normal use of the pipelines, and even cause major safety accidents.

Reasonable evaluation of pipeline deformation is essential for the design and construction of shield tunneling projects, which has attracted attention of many scholars. In terms of theoretical analysis, the elastic foundation beam model was commonly used to analyze the pipeline deformation, among which the Winkler model was the most popular, but it ignored the continuity of foundation deformation (Tanahashi 2004, Carrier *et al*. 2005). Therefore, many researches modified the Winkler model and developed two-parameter models. Typically, the proposed Pasternak model introduced the shear modulus on the basis of the Winkler model, which enabled consideration of the actual shear effect of the soil in the vertical direction (Civalek and Ozturk 2010, Khudayarov *et al*. 2019, Boulefrakh *et al*. 2019, Sae-Long *et al*. 2021).

Field measurement helps to evaluate tunnel safety and verify the design parameters against the measured results. Many scholars examined new and comprehensive monitoring systems with the development of electronic information technology. Xie *et al*. (2017) developed a multisection deformation measurement method for shield tunnel based on terrestrial laser scanner. Yue *et al*. (2021) proposed a tunnel construction real-time monitoring system and pipeline deformation detection system based on artificial intelligence internet, which enabled monitoring of the deformation position and deformation of tunnel and pipeline in real time. Moreover, many researches established 3D numerical models to analyze pipeline deformation or ground surface settlement caused by crossing shield tunnels under different conditions (Ding *et al*. 2017, Mohannadpour *et al*. 2021, Shao *et al*. 2022, An *et al*. 2022). Zhao *et al*. (2022) examined the influence of

*Corresponding author, Professor
E-mail: jwding@seu.edu.cn
[a]Ph.D. Student, E-mail: jiaoning@seu.edu.cn
[b]Ph.D. Student, E-mail: wanxing1994@seu.edu.cn
[c]Ph.D. Student, E-mail: zhangsai@seu.edu.cn
[d]Graduate Student, E-mail: 220203208@seu.edu.cn

ISSN: 2005-307X (Print), 2092-6219 (Online)

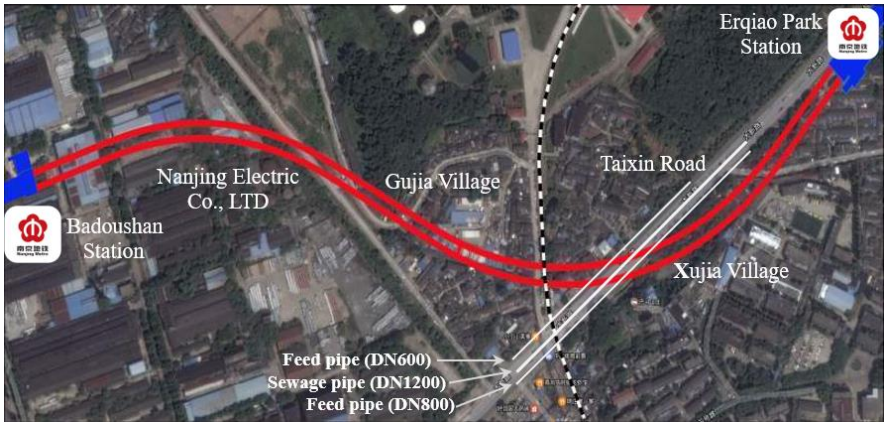

Fig. 1 Location of the project

construction conditions and the included angle between pipeline and tunnel on pipeline deformation. The results indicated that the settlement and deformation area of the pipeline increase as the included angle decreases.

It has been widely accepted that the deformation of the grounds and pipelines are dependent upon stratigraphic conditions, spatial effects (curvature radius, slope and shape of the tunnel), construction parameters and et al. Many scholars studied the ground surface settlement caused by shield tunneling in soft stratum or sand-cobble stratum through numerical simulation, field tests and model tests, found that the surface deformation zone caused by shield tunneling in sandy cobble stratum was smaller than that in soft stratum, and the surface settlement time-history curve presented mutability. (Nagel *et al*. 2010, He *et al*. 2012, Rezaei *et al*. 2019). As for shield tunneling in the soil-rock composite stratum, Ding *et al*. (2021) and Li *et al*. (2020) examined the influence of hard-layer ratio, construction sequence, tunnel spacing on ground surface deformation by field monitoring and numerical simulation. It was found that in the process of crossing the composite strata with different hard-layer ratios, ground surface settlement decreased, but the settlement trough width increased with the hard-layer ratio increased. Moreover, some scholars examined the construction of shield tunneling with large slope and small radius curves through data statistics, numerical simulations and field tests, it is found that the curvature radius and slope of the tunnel played a dominant role in the deformation of ground surface and structures above the tunnel. (Feng *et al*. 2022, Huang and Li 2022). Especially, Deng *et al*. (2021) deduced the deformation prediction equation of the existing pipeline and analyzed the existing pipeline deformation correlated with the shield tunneling along the curved section. Results indicated the deformation of the existing pipeline were asymmetrically distributed, and the settlement of pipeline were negatively correlated with the increase in the tunnel curvature radius.

Currently, the deformation law of pipeline caused by a curved shield tunnel in the soil-rock composite stratum is still unclear. Therefore, a case study of the pipeline deformation was presented based on a double curved shield tunnel in Badoushan-Erqiaopark station of Metro line 1, in the soil-rock composite stratum in Nanjing, China. The stratum settlement equation caused by the double shield tunneling was modified. The effects of hard-layer ratio, turning radius of the tunnel, buried depth of pipeline and et al. on the pipeline deformation were analyzed by numerical simulation. This study can provide reference for the design and construction of similar projects.

2. Project overview

The shield zone from the Badoushan Station to the Erqiao Park Station of Nanjing Metro Line 1 was located in the Qixia District, Nanjing, China. As shown in Fig. 1, the shield tunnels crossed several villages, factories and Taixin Road in sequence, and finally entered the Erqiao Park Station. Note that a concrete DN1200 sewage pipe crossed along Taixin Road with a buried depth of 10.0 m. In addition, a cast-iron DN600 water supply pipeline and a cast-iron DN800 water supply pipeline were buried along both sides of Taixin Road with buried depth of about 3 m.

The shield zone started from K22+037.962 to K23+107.865 with a total length of 1069.903m. The buried depth ranged from 8.1 m to 25.4 m, the distances between two tunnels ranged from 6 m to 10 m. The outer diameter of the lining ring was 6200 mm. The thickness and width of the segment were 350 mm and 1200 mm, respectively. The concrete grade of C50 was used for the segment. The left tunnel was carried out first and then the right tunnel.

The typical cross-section of the shield tunneling along with soil profiles is presented in Fig. 2. The miscellaneous fill and plain fill were distributed in the upper 3.5 m below the surface, followed by a deep silty layer to a depth of 20.8 m. Below the silty layer was a highly weathered sandstone layer with a thickness of 1.8 m, and the lower layer was a moderately weathered sandstone layer.

The plain view of monitoring points of the project as shown in Fig. 3. The distance between each pipeline settlement measuring point and each ground settlement measuring point was about 10 m and 5m, respectively. Due to site limitations and the lack of inspection wells, the indirect deployment method was adopted to bury indirect monitoring points in the soil layer above the pipeline to monitor the settlement of the pipeline.

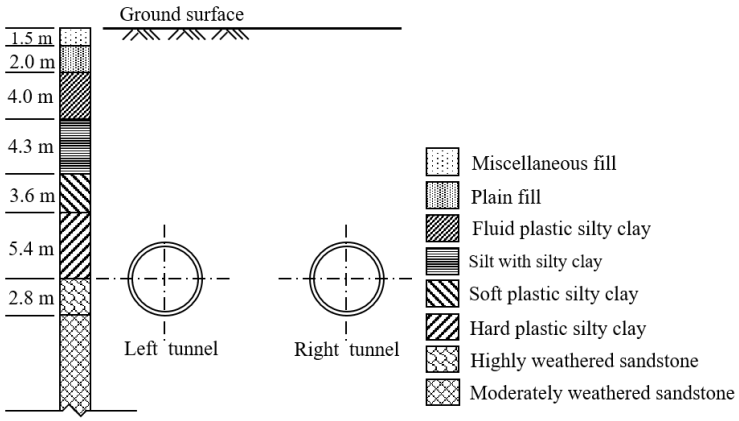

Fig. 2 Typical geological section

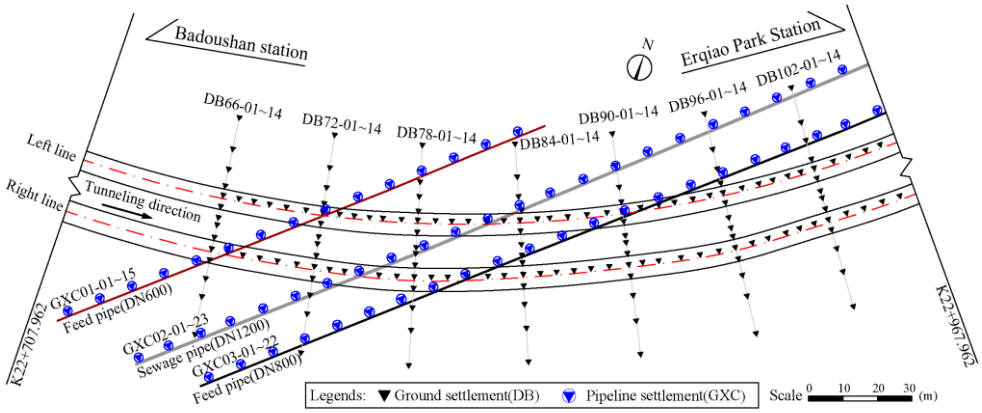

Fig. 3 Plain view of monitoring points

The ground surface settlement measuring points were installed along the longitudinal direction above the tunnel axis. Standard sections were set at the distance of 30 m (25 rings), whose measuring points were located at 2.5 m, 6 m, 11 m, and 25 m away from both sides of the tunnel axis. In addition to comparing the final settlement at each monitoring section, four typical construction stages were selected to compare the settlement at different stages, where stages I and II were for the left tunnel reached and crossed the monitoring section, respectively, and stages III and IV were for the right tunnel reached and crossed the monitoring section, respectively.

3. Results and discussion

3.1 Analysis of monitoring data

The ground surface settlement of three typical monitoring sections with different buried depths of the tunnel (h) as shown in Fig. 4(a). The ground surface settlement and the width of the settlement trough increased gradually with decreasing tunnel depth. It can be observed that the settlement curve changed from V-shaped to W-shaped, and the position of the maximum settlement moved from the upper of the double tunnel central axis to the upper of tunnel axis. Furthermore, the settlement of the upper of the left tunnel was larger than the right one, which was attributed to the secondary disturbance of the stratum around the left tunnel during the right shield tunneling (Zhou *et al.* 2021).

Figs. 4(b) and 4(c) show the surface settlement at different construction stages and the development of ground surface settlement of a cross-section with time, respectively. The ground surface settlement was small before the arrival of the shield machine. The settlement occurred mainly in the middle and later stages of the process when the shield machine passed through the monitoring section. The friction load , radial contraction of the shield shell, and the grouting load of the shield tail caused the soil loss in the later stages, resulting in predominant ground surface settlement. The left shield tunneling had an insignificant influence on the ground surface above the right tunnel. In contrast, the right shield tunneling had an impact on the stratum around the left tunnel, which caused incremental ground surface settlement above the left tunnel remarkably.

The development of pipeline settlement with time as shown in Fig. 5. The settlement development of the pipeline was generally consistent with that of the ground surface. The settlement was smaller before the arrival of the shield machine, but it increased remarkably during the middle and later stages. Fig. 6 shows the pipeline settlement at different

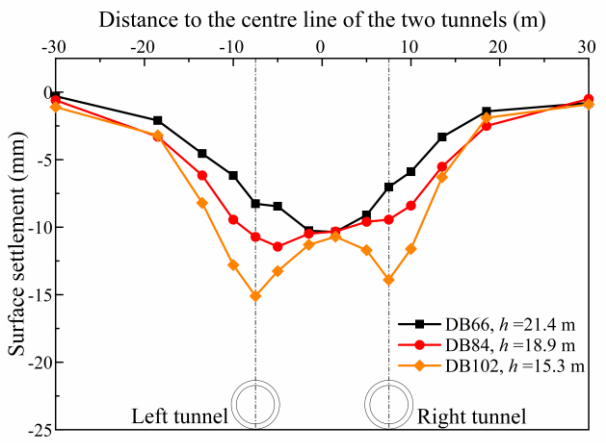

(a) Ground settlement of typical monitoring sections

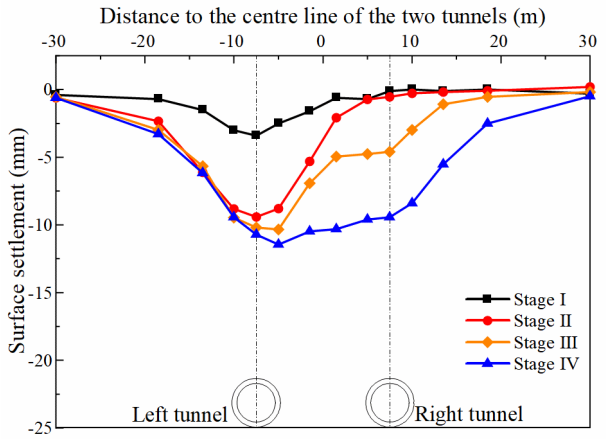

(b) Settlement at different construction stages (DB84)

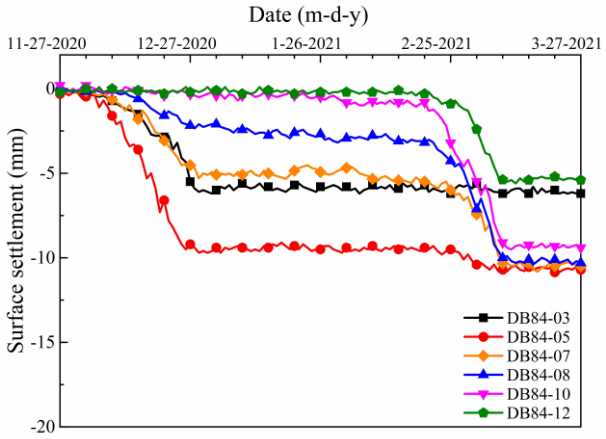

(c) Settlement development with time (DB84)

Fig. 4 Measured data of ground surface settlement

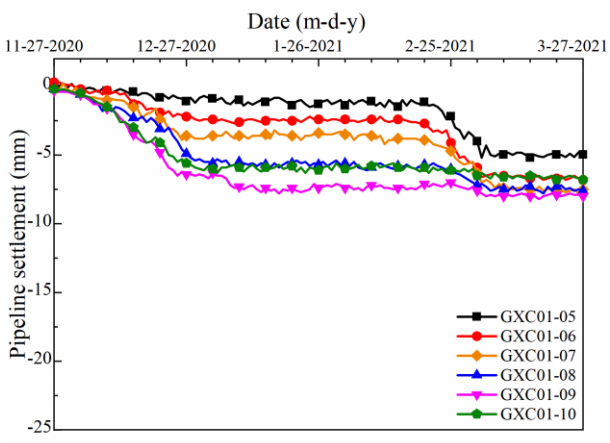

(a) Feed pipe(DN600)

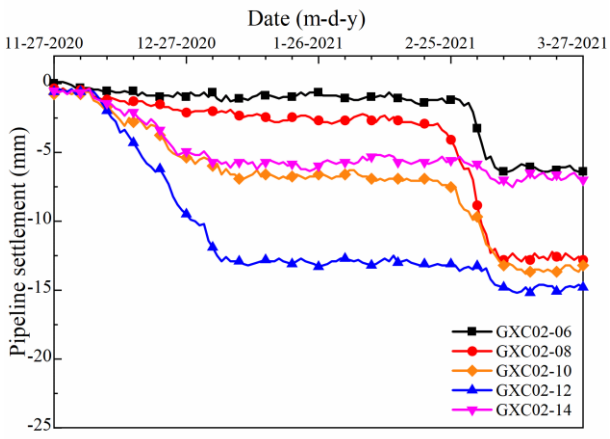

(b) Sewage pipe(DN1200)

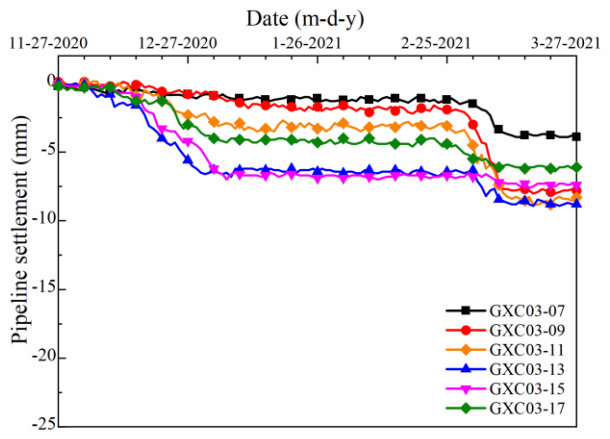

(c) Feed pipe(DN800)

Fig. 5 Settlement development of pipelines with time

construction stages. Since the shield machine crossed the DN600 feed pipe, the DN1200 sewage pipe, and the DN800 feed pipe in sequence, the settlement development process was the earliest for the DN600, and it was the latest for the DN800 feed pipe. The maximum settlement of the DN1200 sewage pipe was approximately 1.5 to 2 times that of the other two pipelines. Moreover, the settlement curve of the sewage pipe was featured with a W-shape with the maximum pipeline settlement located in the upper of the axis of the left tunnel. Differently, the settlement curve of the two feed pipes was characterized by a V-shape with the maximum pipeline settlement located in the upper of the central axis of the double tunnels. The settlement trough width of the DN800 feed pipe was the largest, followed bythe DN1200 sewage pipe and the DN600 feed pipe. The significant differences in the final settlement among the pipelines should be ascribed to the differences in the diameter, material, buried depth of the pipelines, and the

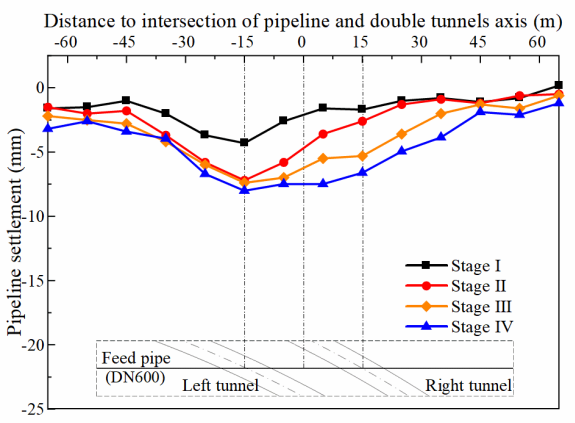

(a) Feed pipe(DN600)

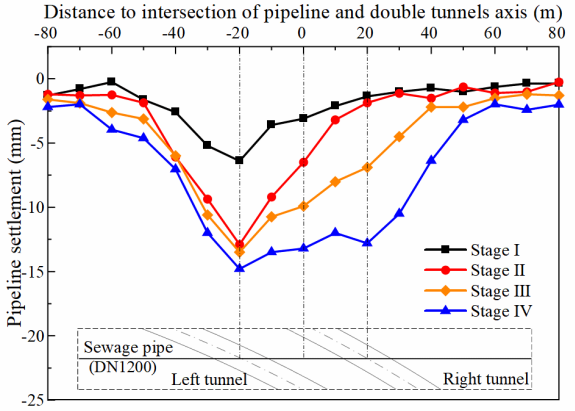

(b) Sewage pipe(DN1200)

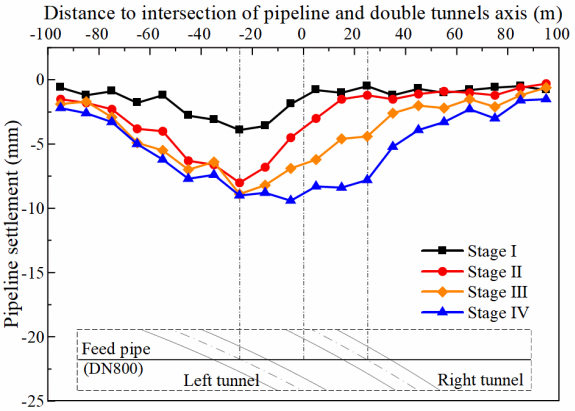

(c) Feed pipe(DN800)

Fig. 6 Settlement curves of pipelines at different construction stages

angle between the pipeline and tunnel axis (Zhao *et al.* 2022).

3.2 Correction of the calculation equation

Ground and pipeline settlement caused by shield tunneling is mainly correlated with the ground loss, stress redistribution, deformation and reconsolidation of disturbed soil (Marshall *et al.* 2010). In addition, in the process of shield tunneling, the surrounding soils will be disturbed by the face thrust, grouting pressure, cutterhead torque, and shield machine vibration. Therefore, it is very complicated to estimate the stratum and pipeline settlement.

Based on massive measured data of ground surface settlement caused by tunneling, Peck (1969) proposed an empirical equation to calculate the ground surface settlement, as shown in Eqs. (1) and (2).

$$S = S_{\max} \exp\left[-\frac{x^2}{2i^2}\right] \tag{1}$$

$$S_{\max} = \frac{V_{loss}}{i\sqrt{2\pi}} = \frac{\pi R^2 \eta}{i\sqrt{2\pi}} \tag{2}$$

Where S*max* denotes the maximum ground surface settlement (S), i denotes the width of the ground surface settlement trough, η denotes the rate of formation loss (V_{loss}). The formation loss rate (η) can be obtained by empirical value, or be back-calculated by Eq. (2) through measured data. The settlement trough width (i) can be calculated by the Eq. (3) (Celestino *et al.* 2020).

$$i = m\left[R + h\tan(45^\circ - \varphi/2)\right] \tag{3}$$

Where m refers to the coefficient ranging from 0.45 to 0.50. R denotes the radius of the tunnel, h denotes the distance from the tunnel axis to surface, φ represents the average internal friction angle of the soil above the tunnel axis.

For the shield tunneling in the soil-rock composite stratum, the properties of rock and soil in each layer are quite different. Hence, the calculated settlement using the settlement calculation Eq. (1) directly is not accurate enough. Ding *et al.* (2021) modified the settlement calculation equation by introducing the ground surface settlement correction coefficient (a) and the settlement trough width correction coefficient (b), as shown in Eq. (4).

$$S = aS_{\max} \exp\left[-\frac{x^2}{2(bi)^2}\right] \tag{4}$$

For the double shield tunnel, the settlement curve is not a simple superposition of the left tunnel and right tunnel considering their interaction. Suwansawat and Einstein (2007) established an improved ground surface settlement prediction equation for the double shield tunneling by the hypergeometric method, as shown in Eq. (5). Where x and L represent the distance to the central axis of the two tunnels and the distance between two tunnel axes, respectively.

Substituting Eqs. (2) and (4) into Eq. (5) yields the Eq. (6), it can calculate the stratum settlement caused by the double shield tunneling in the soil-rock composite stratum.

$$S(x) = S_{\max 1} \exp\left[-\frac{(x-0.5L)^2}{2i_1^2}\right] + S_{\max 2} \exp\left[-\frac{(x+0.5L)^2}{2i_2^2}\right] \tag{5}$$

$$S(x) = \frac{a\pi R^2 \eta_1}{bi_1\sqrt{2\pi}} \exp\left[-\frac{(x-0.5L)^2}{2(bi_1)^2}\right] + \frac{a\pi R^2 \eta_2}{bi_2\sqrt{2\pi}} \exp\left[-\frac{(x+0.5L)^2}{2(bi_2)^2}\right] \tag{6}$$

The soil loss rate and the settlement trough width are used to calculate the settlement without considering the

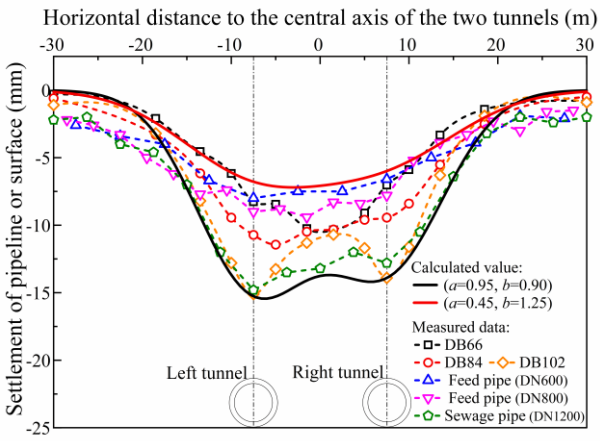

Fig. 7 Comparison between measured data and calculated values by the modified equation

presence or absence of pipelines, hence the equation is still applicable when the pipelines are distributed in the soils (Sun *et al*. 2021). During shield tunneling in the soil-rock composite stratum, the final stratum settlement is relatively small owing to the high stability of the lower strata and the relatively small influence of stratum loss and grouting load, where the pipeline settlement is close to the stratum settlement. Therefore, the modified settlement Eq. (6) can be applied to the settlement calculation of ground surface and pipeline settlement by adjusting the correction coefficient appropriately.

In order to determine the value range of the correction coefficient, the measured data of typical surface and pipeline settlement were compared with the calculated value of the modified equation, as shown in Fig. 7. It can be seen that the measured data of settlement at both ends far away from the tunnel axis was larger than the calculated value, which may be explained by the fact that the influence of curved shield tunneling is ignored in the calculation equation. In addition, the modified settlement calculation equation was consistent with the measured data. The upper and lower limit value of the modified coefficient of the settlement calculation equation was obtained through comparison. The correction coefficient a and b ranged from 0.45 to 0.95 and from 0.90 to 1.25 respectively. For the ground surface settlement and pipeline settlement at different locations, the value of the correction coefficient can be determined according to the tunnel depth, pipeline depth, material and pipeline diameter, and other factors.

4. Numerical simulation analysis

4.1 Model establishment

A 3D finite element model was established based on the typical sections of the shield tunnel construction project using Plaxis 3D software. The main steps are as follows.

1. The Length (X direction) × Width (Y direction) × Height (Z direction) of the 3D model was 200.0 m ×100.0 m × 50.0 m, as shown in Fig. 8(a).

2. Different levels of soil stratigraphy were defined. The soil layer and the rock layer were simulated using the Hardening model of Small Strain (HSS) and the Mohr-Coulomb (MC) model, respectively. The physical and mechanical parameters of the soil were obtained from the geological survey report of the site, which involved on-site sampling followed by laboratory tests, as shown in Table 1 (Roboski, 2001, Nawel and Salah 2015, Sarfarazi and Tabaroei 2020, Heama *et al*. 2021).

3. Lateral boundaries were restricted for horizontal movement and the bottom boundary was restricted for both horizontal and vertical movement. But the upper boundary of the model was set as a free boundary.

4. The shield machine, tunnel and pipelines were set, as shown in Fig. 8(b). They were regarded as elastic materials and were modeled using plate plate units. Their physical and mechanical parameters are shown in Table 2. The "interface units" were set up to simulate slab-soil interactions.

5. The equilibrium pressure at the excavation face (P_0), grouting pressure, and jack thrust at the shield tail were applied. The equilibrium pressure at the excavation face was calculated according to the Eq. (7).

$$P_0 = \sum_{i=1}^{n} (1 - \sin\varphi')\gamma_i h_i \tag{7}$$

Where γ_i and h_i represent the weight and the thickness of layer i soil, φ' denotes the internal friction angle.

According to the statistics of the parameters of the field construction, it was known that the jack thrust was 800 kPa, and the grouting pressure at the shield tail was approximately 1.1 to 1.2 times the equilibrium pressure at the excavation face. On the basis of the stratigraphic parameters in Table 1, the equilibrium pressure at the excavation surface was calculated to be 120 kPa, which increased with depth at a rate of 15 kPa/m. The grouting pressure was taken as 140 kPa and increased with depth according to the law of 18 kPa/m.

6. The finite element mesh was generated. The model consisted of 245,809 ten-node tetrahedral with 388,493 nodes.

7. The stage construction model was established. Besides the initial phase, the construction of 120 ring segments with a width of 1.2 meters for left and right tunnels was simulated, respectively. In order to simplify the calculations and shorten the simulation time, three ring segments of excavation and support were simulated for each phase.

8. Calculations were performed until the left and right tunnels were built in sequence.

4.2 Validation by field data

The comparison of the calculated pipeline settlement through numerical simulation and the measured data is presented in Fig. 9. It was found that the measured settlement of the pipeline above the left tunnel was slightly larger than the simulation result. The secondary disturbance caused from the right shield tunneling may be responsible for the difference, which was not considered in the

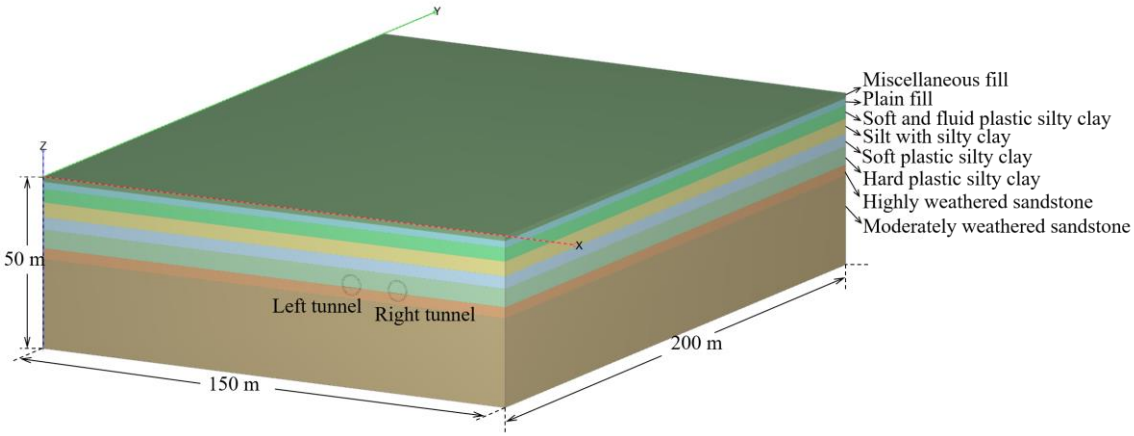

(a) Stratigraphic distribution

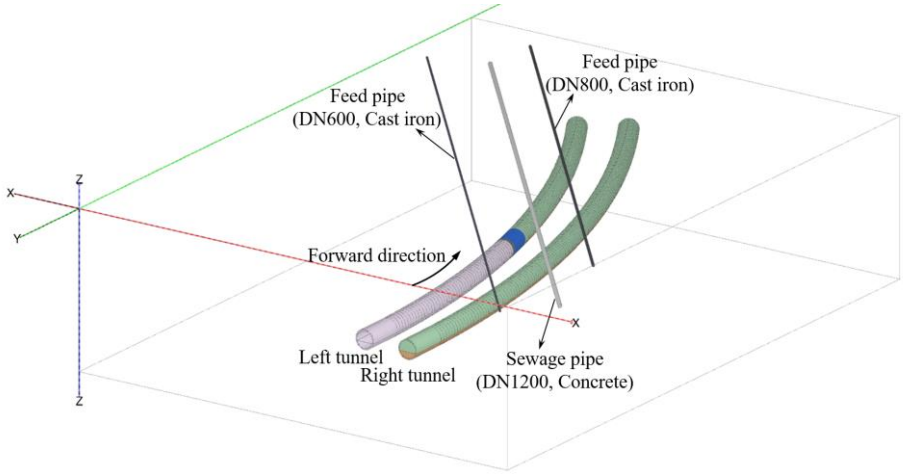

(b) Distribution of tunnels and pipelines

Fig. 8 3D numerical model

Table 1 Physical and mechanical properties of stratum

Soil Materials	Thickness (m)	Gravity (kN/m^3)	Cohesion (kPa)	Internal friction angle (°)	Elastic modulus (Mpa)				Stress index
					E_{50}^{ref}	E_{oed}^{ref}	E_{ur}^{ref}	G_0^{ref}	
Miscellaneous fill	1.5	18.4	18.0	12.0	6.1	5.1	31.6	47.4	0.5
Plain fill	2.0	18.5	15.0	11.6	6.2	5.2	31.2	46.8	0.5
Fluid plastic silty clay	4.0	19.1	18.0	17.1	5.9	5.9	29.7	44.6	0.8
Silt with silty clay	4.3	19.2	10.0	29.4	8.6	8.6	43.0	64.4	0.5
Soft plastic silty clay	3.6	19.1	28.0	18.0	6.3	6.3	31.7	47.5	0.8
Hard plastic silty clay	5.4	19.6	36.0	22.8	8.5	8.5	42. 5	63.7	0.8
Highly weathered sandstone	1.8	25.7	80.0	45.0	200.0				--
Moderately weathered sandstone	--	26.0	900.0	42.0	4140.0				--

*E_{50}^{ref}: Secant modulus; E_{oed}^{ref}: Tangent modulus; E_{ur}^{ref}: Unloading elastic modulus; G_{r0}^{re}: Shear modulus

Table 2 Mechanics Parameters of Structural Members

Structural members	Thickness (mm)	Gravity (kN/m^3)	Elastic modulus (Gpa)	Shear modulus (Gpa)	Poisson ratio
Shield tunneling machine	350	120	23	11.5	0
Shield segment	350	27	31	15.5	0.1
Feed pipe (DN600)	9.9	73	120	60	0.3
Feed pipe (DN800)	11.7	73	120	60	0.3
Sewage pipe (DN1200)	120	25	28	12	0.2

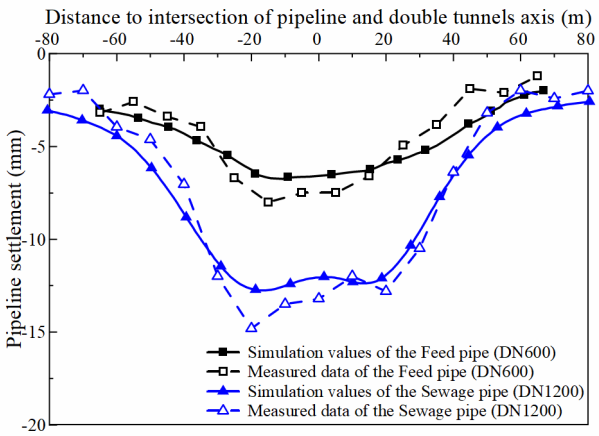

(a) Comparison of settlement values

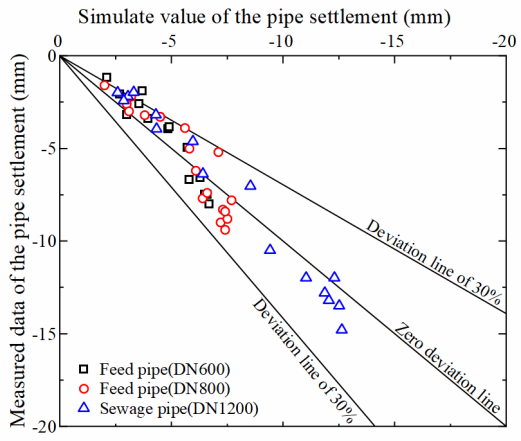

(b) Comparison of deviation value

Fig. 9 Comparison between numerical simulation values and measured data

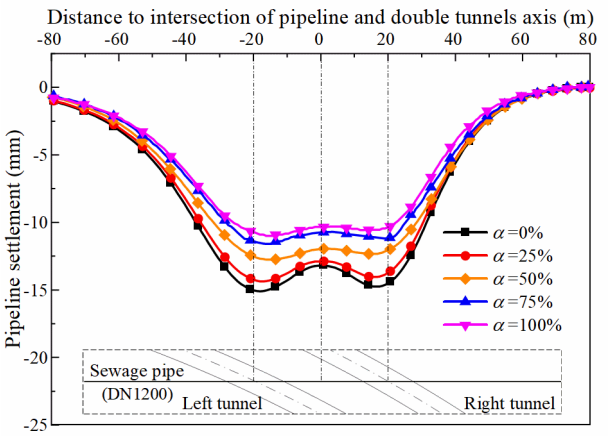

(a) Pipeline settlement

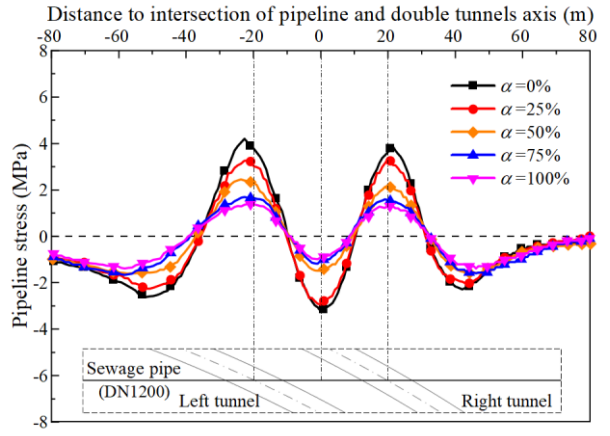

(b) Pipeline stress

Fig. 10 Pipeline settlement and stress with different hard-layer ratios

numerical simulation. The difference between the numerical simulation and the measured data was within 30%, except for some individual points with small settlements. Therefore, the established numerical model is believed to be rational with acceptable error from the field data.

4.3 Parametric analysis

4.3.1 Hard-layer ratio

The distribution of soil and rock layers on the tunneling face varies considerably in the soil-rock composite stratum. The hard-layer ratio α, was defined as the ratio of hard-rock layer thickness to tunnel diameter within the range of the tunnel face (Ding *et al*. 2021). Fig. 10 compared the final settlement and stress distribution of the pipeline at different hard-layer ratios.

As shown in Fig. 10(a), the settlement curves gradually changed from W-shape to U-shape as the hard-layer ratio increased. Furthermore, the pipeline settlement decreased remarkably, and the maximum settlement reduced by 29.8% as the hard-layer ratio increased from 0% to 100%. In contrast, the settlement trough width was nearly unchanged. As shown in Fig. 10(b), the pipeline located at the upper part of the tunnel axis was subjected to tensile stress, but that located on the upper part of the central axis of the double tunnels and the pipeline on both sides of the tunnel were subjected to compressive stress. Thus, the pipeline was subjected to uneven stress. It is inferred that the pipeline above the tunnel axis was prone to tensile damage owing to the far lower tensile strength of the concrete pipe than the compressive strength. The stress unevenness and the maximum stress of the pipeline gradually reduced by increasing hard-layer ratio. The maximum tensile stress of pipeline decreased from 4.2 MPa to 1.39 MPa with incremental hard-layer ratio from 0% to 100%.

Therefore, the settlement of the pipeline was relatively larger and the stress unevenness was more obvious when the hard-layer ratio was smaller, and the part of the pipeline located above the tunnel axis was vulnerable to tensile damage. The pipeline deformation caused by shield construction gradually decreased with increasing hard-layer ratio, but the influence range on the pipeline was almost unchanged.

4.3.2 Tunnel curvature radius

The comparison of final settlement and stress of the pipeline with different tunnel curvature radii (R_T) as shown in Fig. 11. It can be seen from Fig. 11(a), the settlement trough width caused by shield construction gradually decreased with the increasing curvature radius, but the

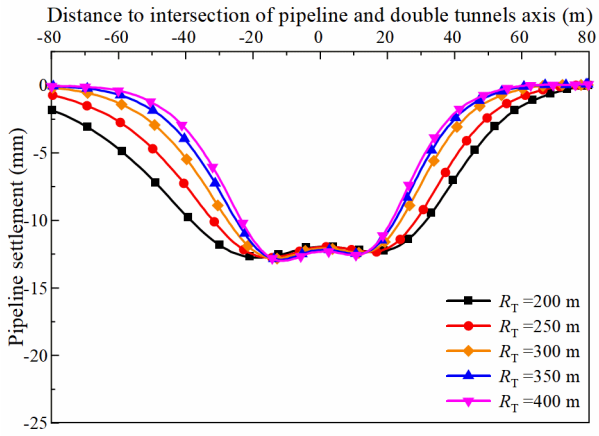

(a) Pipeline settlement

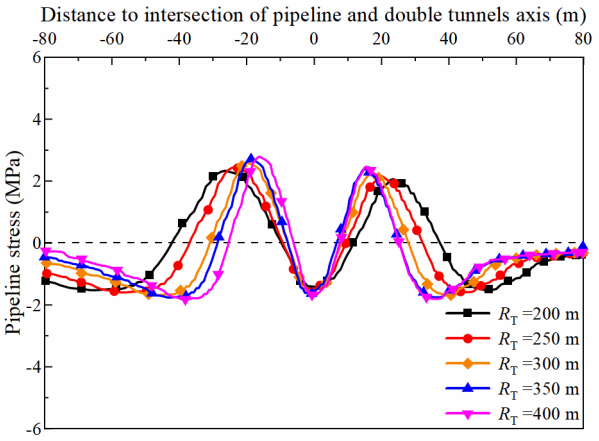

(b) Pipeline stress

Fig. 11 Pipeline settlement and stress with different tunnel curvature radius

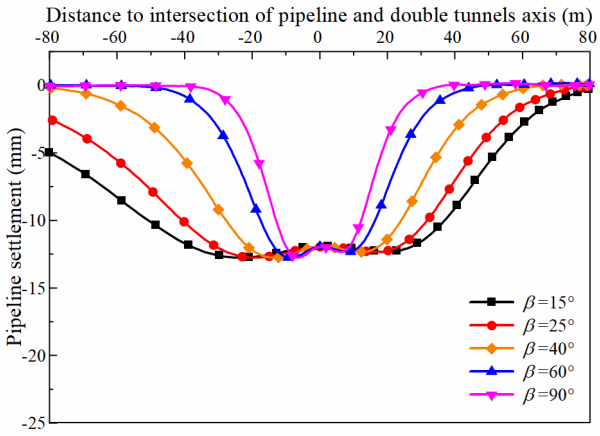

(a) Pipeline settlement

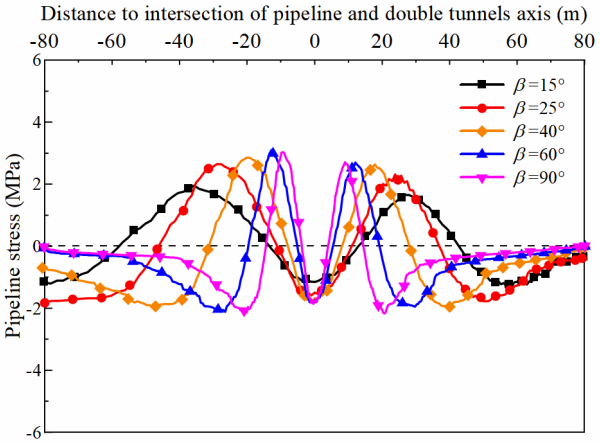

(b) Pipeline stress

Fig. 12 Pipeline settlement and stress with different included angle between pipeline and tunnel axis

decreasing rate gradually slowed down. It is noticed that, the maximum settlement of the pipeline was nearly unchanged with varying tunnel curvature radii, whose location was found to be above the tunnel axis invariably. The pipeline settlement were asymmetrically distributed on both sides of the tunnel, and the differences decreased gradually with the increasing curvature radius.

As shown in Fig. 11(b), the pipeline located at the upper part of the tunnel axis was subjected to tensile stress, but the other parts were subjected to compressive stress. The length of pipeline subjected to tensile stress gradually decreased with the increasing curvature radius. In contrast, the tensile stress increased slightly, resulting in more concentrated stress of the pipeline.

The included angle between pipeline and tunnel axis varies with the tunnel curvature radius. However, the variation range of the included angle (β) is wider owing to the complexity of the surrounding pipelines in urban shield construction. The final settlement and stress of the pipeline with different included angles (β) is presented in Fig. 12. The included angle between pipeline and tunnel axis had similar effects on pipeline deformation with the tunnel curvature radius. The settlement trough width, maximum stress and the length subjected to tensile stress of the pipeline decreased with the increasing included angle, but the maximum settlement of the pipeline was nearly unchanged. Moreover, the position of the maximum settlement and maximum stress of the pipeline moved towards the upper part of the tunnel axis gradually.

Therefore, the length of pipeline deformation caused by shield tunneling decreases as the tunnel curvature radius or the included angle between pipeline and tunnel axis increases. However the settlement and stress of the pipeline becomes more concentrated, which poses a great threat to the pipeline safety.

4.3.3 Pipeline buried depth

The final settlement and stress of the pipeline with different pipeline buried depths (H) is presented in Fig. 13. As shown in Fig. 13(a), the settlement of the pipeline within 40 m from the central axis gradually increased as the pipeline buried depth increased, but the settlement trough width of the pipeline decreased slightly. Moreover, the settlement curve changed from V-shaped to W-shaped, and the position of the maximum settlement moved from the upper of the double tunnel central axis to the upper of tunnel axis.

As shown in Fig. 13(b), the stress of the pipeline

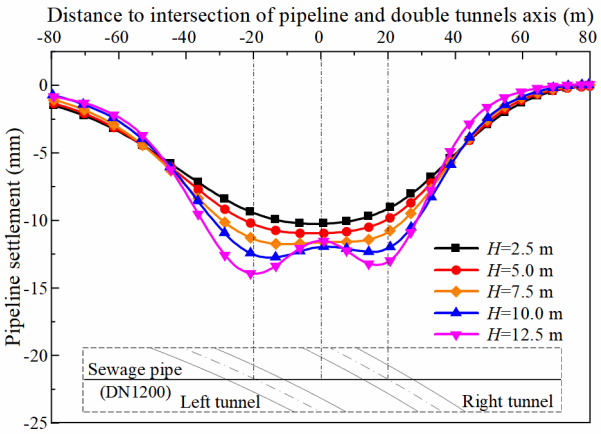

(a) Pipeline settlement

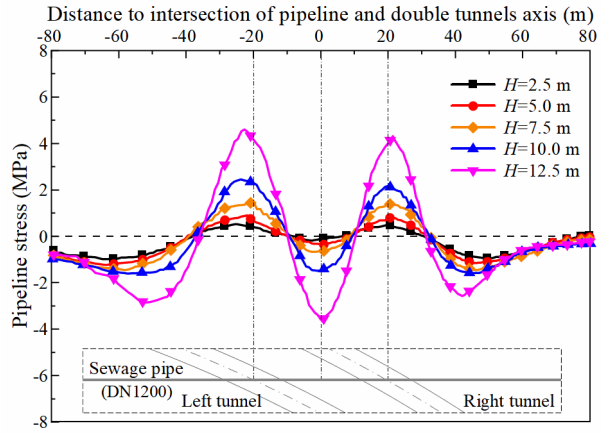

(b) Pipeline stress

Fig. 13 Pipeline settlement and stress with different buried depth of pipeline

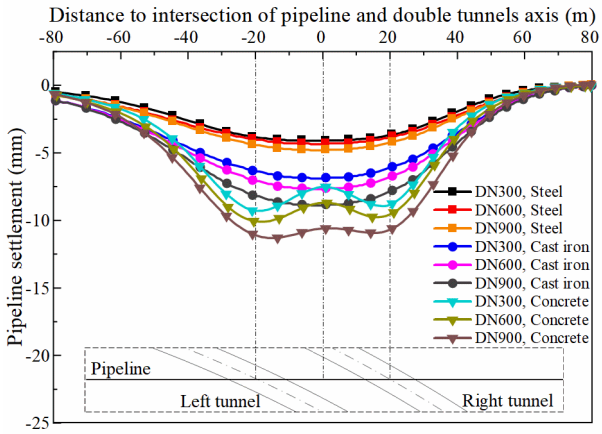

(a) Pipeline settlement

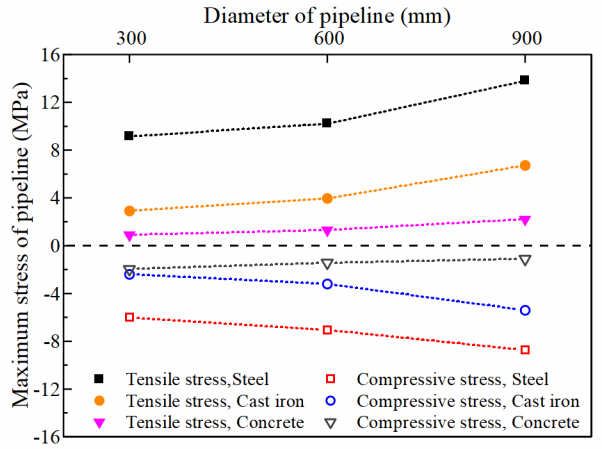

(b) Maximum stress of pipeline

Fig. 14 Pipeline settlement and stress with different material and diameter of pipeline

increased with the increasing pipeline buried depth, which was proportional to the settlement of the pipeline. The maximum tensile and compressive stresses of the pipeline was 4.86 MPa and 3.68 MPa, respectively. The pipeline was considered to be in a stable state with the maximum stress within the allowable limit.

Therefore, the pipeline deformation was positively correlated with the buried depth of pipeline. As the pipeline buried depth increases, the settlement of the pipeline increases and the stress becomes more uneven.

4.3.4 Material and diameter of pipeline

The materials and diameters of the urban municipal pipelines vary considerably. Three elastic modulus of 28 Gpa (Concrete), 120 Gpa (Cast iron) and 210 Gpa (Steel) and three pipeline diameters of 300 mm, 600 mm and 900 mm were selected for the numerical simulation.

The final settlement and the maximum stress of the pipeline with different materials and diameters as shown in Fig. 14. It can be seen from Fig. 14(a), the concrete pipe underwent the largest settlement, followed by the cast iron pipe and the steel pipe. The settlement curves of the cast iron pipes and the steel pipes were V-shaped, but the concrete pipes had W-shaped settlement curves. Therefore, the settlement of the pipeline decreased with the increasing elastic modulus of the pipeline, and the settlement curve of pipeline changed from W-shaped to V-shaped gradually. Moreover, the settlement of the pipeline increased with the pipeline diameter, with the smallest increase for steel pipes and the largest increase for concrete pipes. The maximum settlement of the concrete pipe increased by 27.6% as the pipeline diameter increased from 300 mm to 900 mm.

As shown in Fig. 14(b), the maximum pipeline stress of three materials increased with the pipeline diameter, except for the compressive stress in the concrete pipe. The different law of it was attributed to the changing settlement curve of concrete pipe from V-shaped to W-shaped with the decreasing pipeline diameter, which results in larger compressive stress in the lower part of the pipeline above the central axis of the double tunnels. Steel pipe had the smallest settlement but the largest stress, which should be attributed to its large elasticity modulus and small wall thickness. The maximum tensile and compressive stresses of steel pipe was 13.8 MPa and 8.7 MPa respectively, but the maximum allowable stress of the steel pipe was over 300 MPa, much greater than the maximum stress of the steel pipe, it was still in a stable state.

Therefore, the shield tunneling had a greater impact on

Table 3 Relative sensitivity of each factor

	Relative sensitivity	
	Settlement of pipeline	Width of pipeline settlement trough
Hard-layer ratio	0.150	0.088
Tunnel curvature radius	0.031	0.366
Angle between pipeline and tunnel axis	0.018	0.156
Buried depth of pipeline	0.119	0.042
Diameter of pipeline	0.091	0.043
Elastic modulus of pipeline	0.106	0.029

the deformation of the concrete pipeline, and the settlement and stress of the pipeline increased with the pipeline diameter.

4.4 Sensitivity analysis of parameters

The relative sensitivity analysis was used to analyze the influence magnitude of the parameters on pipeline deformation, the basic principle of which is as follows

$$\eta_{SR} = \frac{\left[\frac{f(x_{LR}) - f(x)}{f(x)}\right] \times 100\%}{\left[\frac{x_{LR} - x}{x}\right] \times 100\%} \tag{8}$$

Sensitivity factor η_{SR}, was defined as the rate of percentage of output divided by the percentage of a parameter, where x and x_{LR} represent the input variables, $f(x)$ and $f(x_{LR})$ denote the corresponding output, as shown in the Eq. (8).

Sensitivity coefficient η_{SS}, is an expansion of the η_{SR} and a more significant way to assess the source of uncertainty, obtained by multiplying the regularized rate of input variable, as shown in the Eq. (9).

$$\eta_{SS} = \eta_{SR} \times \frac{\left[\max(x_R) - \min(x_R)\right]}{x} \tag{9}$$

Where $\max(x_R)$ and $\min(x_R)$ denote the maximum and minimum values of the parameter variation respectively.

The relative sensitivity, $a(x_i)$, to individual calculation results was introduced, which can compare the sensitivity of different parameters, as shown in Eq. (10), in which, n is the number of parameter variables.

$$a(x_i) = \frac{\eta_{ss_i}}{\sum_{i=1}^{n} \eta_{ss_i}} \tag{10}$$

The relative sensitivity of each parameter on the deformation of the pipeline as shown in Table 3. It can be seen that the most influential parameter on the settlement of the pipeline was the hard-layer ratio, followed by the buried depth and the elastic modulus of the pipeline, and the least influential was the included angle between pipeline and tunnel axis. The tunnel curvature radius and the included angle between pipeline and tunnel axis had the greatest impact on the settlement trough width of the pipeline, the impact of other parameters was essentially small.

Therefore, in the design of the shield tunnel that crosses pipelines in soil-rock composite stratum, the buried depth of the tunnel should be increased appropriately to increase the hard-layer ratio in the tunnel face. The tunnel curvature radius and the included angle between pipeline and tunnel should be increased properly to reduce the deformation scope of the pipeline.

5. Conclusions

The influence of double curved shield in the soil-rock composite stratum on the pipeline deformation was investigated with field measurement and numerical simulation in this study. The main conclusions are as follows.

- The subsequent shield tunnel would cause secondary disturbance to the soil around the preceding tunnel, resulting in increased pipeline and ground surface settlement above the preceding tunnel.
- The modified settlement calculation equation was consistent with the measured data. It can be applied to the settlement calculation of ground surface and pipeline settlement, the modified coefficients a and b ranged from 0.45 to 0.95 and 0.90 to 1.25, respectively.
- When the hard-layer ratio was smaller or the pipeline buried depth was bigger, the settlement of the pipeline was relatively larger and the stress unevenness was more obvious. Consequently, the part of the pipeline located above the tunnel axis was vulnerable to tensile damage.
- The settlement and stress of the pipeline becomes more concentrated as the tunnel curvature radius or the included angle between pipeline and tunnel axis increases, which poses a great threat to the pipeline safety. Shield tunneling had a greater impact on the deformation of the pipeline made of concrete, and the pipeline deformation increased with pipeline diameter.
- The hard-layer ratio had the most significant impact on the pipeline settlement. The tunnel curvature radius and the angle between pipeline and tunnel axis played a predominant role in the scope of the pipeline settlement deformation.

Acknowledgments

The research described in this paper was partially supported by the National Natural Science Foundation of China (Grant No. 51978159) and the National Key R&D Program of China (Grant No. 2015CB057803).

References

An, J.B., Kang, S.J., Kim, J. and Cho, G.C. (2022), "Numerical evaluation of surface settlement induced by ground loss from the face and annular gap of EPB shield tunneling", *Geomech. Eng.*, **29**(3), 291-300. https://doi.org/10.12989/gae.2022.29.3.291.

Boulefrakh, L., Hebali, H., Chikh, A., Bousahla, A.A., Tounsi, A. and Mahmoud, S.R. (2019), "The effect of parameters of visco-Pasternak foundation on the bending and vibration properties of a thick FG plate", *Geomech. Eng.*, **18**(2), 161-178. https://doi.org/10.12989/gae.2019.18.2.161.

Carrier III, W.D. (2005), "Pipeline supported on a nonuniform Winkler soil model", *J. Geotech. Geoenviron. Eng.*, **131**(10), 1301-1304. https://doi.org/10.1061/(ASCE)1090-0241(2005)131:10(1301).

Celestino, T.B., Gomes, R.A.M.P. and Bortolucci, A.A. (2000), "Errors in ground distortions due to settlement trough adjustment", *Tunn. Undergr. Sp. Technol.*, **15**(1), 97-100. https://doi.org/10.1016/S0886-7798(99)00054-1.

Civalek, O. and Ozturk, B. (2010), "Free vibration analysis of tapered beam-column with pinned ends embedded in Winkler-Pasternak elastic foundation", *Geomech. Eng.*, **2**(1), 45-56. https://doi.org/10.12989/gae.2010.2.1.045.

Deng, H., Fu, H., Shi, Y., Huang, Z. and Huang, Q. (2021), "Analysis of asymmetrical deformation of surface and oblique pipeline caused by shield tunneling along curved section", *Symmetry*, **13**(12), 2396. https://doi.org/10.3390/sym13122396.

Ding, Z., Wei, X.J. and Wei, G. (2017), "Prediction methods on tunnel-excavation induced surface settlement around adjacent building", *Geomech. Eng.*, **12**(2), 185-195. https://doi.org/10.12989/gae.2017.12.2.185.

Ding, J., Zhang, S., Zhang, H., Guo, C., Liao, Z. and Liu, H. (2021), "Ground settlement caused by shield tunneling in soil-rock composite strata", *J. Perform. Constr. Fac.*, **35**(5), 04021057. https://doi.org/10.1061/(ASCE)CF.1943-5509.0001631.

Feng, X., Wang, P., Liu, S., Wei, H., Miao, Y. and Bu, S. (2022), "Mechanism and law analysis on ground settlement caused by shield excavation of small-radius curved tunnel", *Rock Mech. Rock Eng.*, **55**(6), 3473-3488. https://doi.org/10.1007/s00603-022-02819-6.

He, C., Feng, K., Fang, Y. and Jiang, Y. (2012), "Surface settlement caused by twin-parallel shield tunnelling in sandy cobble strata", *J. Zhejiang Univ. Sci. A*, **13**(11), 858-869. https://doi.org/10.1631/jzus.A12ISGT6.

Huang, C. and Li, S. (2022), "Influence analysis on the excavation of the large-slope shield tunnel in the Guang-zhou-Shenzhen-Hong Kong Express Rail Link", *Arabian J. Geosci.*, **15**, 991. https://doi.org/10.1007/s12517-022-10207-1.

Heama, N., Jongpradist, P., Lueprasert, P., Suwansawat, S. and Jamsawang, P. (2021), "Comparative effects of adjacent loaded pile row on existing tunnel by 2D and 3D simulation models", *Geomech. Eng.*, **27**(2), 151-165. https://doi.org/10.12989/gae.2021.27.2.151.

Jeon, Y.J., Jeon, S.C., Jeon, S.J. and Lee, C.J. (2020), "Study on the behaviour of pre-existing single piles to adjacent shield tunnelling by considering the changes in the tunnel face pressures and the locations of the pile tips", *Geomech. Eng.*, **21**(2), 187-200. https://doi.org/10.12989/gae.2020.21.2.187.

Jin, D., Yuan, D., Li, X. and Zheng, H. (2018), "Analysis of the settlement of an existing tunnel induced by shield tunneling underneath", *Tunn. Undergr. Sp. Technol.*, **81**, 209-220. https://doi.org/10.1016/j.tust.2018.06.035.

Khudayarov, B.A., Komilova, K. M. and Turaev, F.Z. (2019), "The effect of two-parameter of Pasternak foun-dations on the oscillations of composite pipelines conveying gas-containing fluids", *Int. J. Press. Vess. Piping*, **176**, 103946. https://doi.org/10.1016/j.ijpvp.2019.103946.

Koyama, Y. (2003), "Present status and technology of shield tunneling method in Japan", *Tunn. Undergr. Sp. Technol.*, **18**(2-3), 145-159. https://doi.org/10.1016/S0886-7798(03)00040-3.

Li, L., Du, X. and Zhou, J. (2020), "Numerical simulation of site deformation induced by shield tunneling in typical upper-soft-lower-hard soil-rock composite stratum site of changchun", *KSCE J. Civil Eng.*, **24**(10), 3156-3168. https://doi.org/10.1007/s12205-020-0124-0.

Marshall, A.M., Klar, A. and Mair, R.J. (2010), "Tunneling beneath buried pipes: view of soil strain and its effect on pipeline behavior", *J. Geotech. Geoenviron. Eng.*, **136**(12), 1664-1672. https://doi.org/10.1061/(ASCE)GT.1943-5606.0000390.

Mohannadpour, R. and Taheri, E. (2021), "Effect of excavation shield conicality on displacement and stress on the pipeline in layered areas during pipe jacking operations", *Tunn. Undergr. Sp. Eng.*, **10**(3), 271-285. https://doi.org/10.22044/TUSE.2022.11623.1446.

Nawel, B. and Salah, M. (2015), "Numerical modeling of two parallel tunnels interaction using three-dimensional finite elements method", *Geomech. Eng.*, **9**(6), 775-791. https://doi.org/10.12989/gae.2015.9.6.775.

Nagel, F., Stascheit, J. and Meschke, G. (2010), "Process-oriented numerical simulation of shield-supported tunnelling in soft soils", *Geomech. Tunnelling*, **3**(3), 268-282. https://doi.org/10.1002/geot.201000024.

Peck, R.B. (1969), "Deep excavations and tunneling in soft ground", *Proceedings of the 7th International Conference on Mechanics and Foundation Engineering*, Mexico City, Mexico.

Qian, W., Huang, M., Sun, C., Huang, B., Wang, G. and Liu, H. (2021), "Adaptability of earth pressure balance shield tunneling in coastal complex formations: a new evaluation method", *Geomech. Eng.*, **27**(4), 375-390. https://doi.org/10.12989/gae.2021.27.4.375.

Rezaei, A.H., Shirzehhagh, M. and Golpasand, M.R.B. (2019), "EPB tunneling in cohesionless soils: A study on Tabriz Metro settlements", *Geomech. Eng.*, **19**(2), 153-165. https://doi.org/10.12989/gae.2019.19.2.153.

Roboski, J.F. (2001), "Soil parameters for constitutive models of compressible Chicago glacial clays", Ph.D. Dissertation, Northwestern University, Evanston.

Sae-Long, W., Limkatanyu, S., Hansapinyo, C., Prachasaree, W., Rungamornrat, J. and Kwon, M. (2021), "Nonlinear flexibility-based beam element on Winkler-Pasternak foundation", *Geomech. Eng.*, **24**(4), 371-388. https://doi.org/10.12989/gae.2021.24.4.371.

Sarfarazi, V. and Tabaroei, A. (2020), "Numerical simulation of the influence of interaction between Qanat and tunnel on the ground settlement", *Geomech. Eng.*, **23**(5), 455-466. https://doi.org/10.12989/gae.2020.23.5.455.

Shao, X., Yang, Z., Jiang, Y., Yang, X. and Qi, W. (2022), "Field test and numerical study of the effect of shield tail-grouting parameters on surface settlement", *Geomech. Eng.*, **29**(5), 509-522. https://doi.org/10.12989/gae.2022.29.5.509.

Sun, S., Rong, C., Wang, H., Cui, L. and Shi, X. (2021), "The ground settlement and the existing pipeline response induced by the nonsynchronous construction of a twin-tunnel", *Adv. Civil Eng.*, **2021**, 8815304. https://doi.org/10.1155/2021/8815304.

Suwansawat, S. and Einstein, H.H. (2007), "Describing settlement troughs over twin tunnels using a superposition technique", *J. Geotech. Geoenviron. Eng.*, **133**(4), 445-468. https://doi.org/10.1061/(ASCE)1090-0241(2007)133:4(445).

Tanahashi, H. (2004), "Formulas for an infinitely long Bernoulli-Euler beam on the Pasternak model", *Soils Found.*, **44**(5), 109-118. https://doi.org/10.3208/sandf.44.5_109.

Xie, X. and Lu, X. (2017), "Development of a 3D modeling algorithm for tunnel deformation monitoring based on terrestrial laser scanning", *Underground Sp.*, **2**(1), 16-29. https://doi.org/10.1016/j.undsp.2017.02.001.

Xue, Y., Li, X., Qiu, D., Ma, X., Kong, F., Qu, C. and Zhao, Y. (2019), "Stability evaluation for the excavation face of shield tunnel across the Yangtze River by multi-factor analysis",

Geomech. Eng., **19**(3), 283-293. https://doi.org/10.12989/gae.2019.19.3.283.

Yue, Z., Sun, H., Zhong, R. and Du, L. (2021), "Method for tunnel displacements calculation based on mobile tunnel monitoring system", *Sensors*, **21**(13), 4407. https://doi.org/10.3390/s21134407.

Zhang, Z.G., Zhao, Q.H. and Zhang, M.X. (2016), "Deformation analyses during subway shield excavation considering stiffness influences of underground structures", *Geomech. Eng.*, **11**(1), 117-139. https://doi.org/10.12989/gae.2016.11.1.117.

Zhao, S.W., Li, X.L., Li, X., Chen, L.G., Li, T., Li, S.H. and Bai, Y. (2022), "Analysis of pipeline deformation caused by shield tunnel excavation that obliquely crosses existing pipelines", *Arabian J. Geosci.*, **15**(3), 1-14. https://doi.org/10.1007/s12517-022-09462-z.

Zhou, Zh., Ding, H., Miao L. and Gong, C. (2021), "Predictive model for the surface settlement caused by the excavation of twin tunnels", *Tunn. Undergr. Sp. Technol.*, **114**, 104014. https://doi.org/10.1016/j.tust.2021.104014.

CC